

Paper:

Fluid-Structure Interaction Analysis of a Soft Robotic Fish Using Piezoelectric Fiber Composite

Wenjing Zhao, Aiguo Ming, Makoto Shimojo, Yohei Inoue, and Hiroshi Maekawa

Department of Mechanical Engineering and Intelligent Systems, The University of Electro-Communications

1-5-1 Chofugaoka, Chofu-shi, Tokyo 182-8585, Japan

E-mail: zhaowenjing@rm.mce.ucc.ac.jp

[Received March 28, 2014; accepted August 22, 2014]

Designing a high-performance soft robotic fish requires considering the interaction between the flexible robot structure and surrounding fluid. This paper introduces fluid-structure interaction (FSI) analysis used to enhance the hydrodynamic performance of soft robotic fish using piezoelectric fiber composite (PFC) as the propulsion actuator. The basic FSI analysis scheme for soft robotic fish is presented, then the numerical model of the actuator, robot structure, and surrounding fluid are described based on the FSI analysis scheme. The FSI analysis of the soft robotic fish is performed through these numerical models. To evaluate the effectiveness of FSI analysis, coupling simulation and experimental results are compared. We found that the calculated results of propulsive force and deformation displacement were similar to those for experiments. These results suggest that FSI analysis is useful and is applicable to evaluating propulsion characteristics of the soft robotic fish to improve performance.

Keywords: biomimetic robotic fish, soft robot, piezoelectric fiber composite (PFC), fluid-structure interaction (FSI), propulsion performance

1. Introduction

With the development of interdisciplinary sciences, including electronic information and biological technology, biomimetic robots contribute much to deal with the problems encountered in human life [1–4]. Many researchers have concentrated on biomimetic robots, for example, especially on the development of biomimetic robotic fish mimicking real fish [4–11]. Examples include Robotuna by MIT, rigid-tailed robotic fish by MSU, Nanyang Awana (NAF-I) by Nanyang Technological University, snake-like robot AmphiBot by EPFL and HELIX-I by TIT, lamprey-like robot by SSSA, FILOSE robot by Tallinn University, London Aquarium's robotic fish by the University of Essex, and robotic eel by the Methran Mojarrad group. In such research, fish are focused on due to their high efficiency, good flexibility, and great maneuverability. Fishlike robots have been applied to seabed

rescue, exploration, and observation and other special underwater tasks [1–5].

The propulsion methodologies of these fishlike robots are classified into motor mechanism [6–10] and artificial muscle mechanisms [11–16]. The motor mechanism is simple but may lack flexibility and have a high energy cost. Robots using motor mechanism have the relatively complex control and tend to be large, heavy and rigid due to use of rigid materials [17]. However, artificial muscle mechanisms can be made soft and flexible by using shape memory alloy (SMA), ionic polymer metal composite (IPMC), electrostatic film, PZT film, giant magnetostrictive alloy (GMA), or PFC. Artificial muscle mechanisms help make robotic fish small and give them relatively smooth propulsion similar to that of real fish.

Due to an incomplete understanding of the swimming mechanisms of real fish [18] and limitations on studies in developing flexible bionic structures and functions with large deformation, the hydrodynamic performance of robotic fish differ from that of real fish and its performance has not been revealed completely due to unestablished hydrodynamic model. Thus, kinematic swimming parameters of robotic fish cannot be controlled well to achieve good mobility and high efficiency. There are, to our knowledge, no published reports on systematic studies of the detailed kinematic swimming performance of robotic fish or their hydrodynamics [19]. Conventional theories, e.g., linearized inviscid flow theory used by Wu [20], large-amplitude elongated-body theory proposed by Lighthill [21], slender-body theory applied by Newman [22], three-dimensional (3-D) waving plate theory developed by Cheng [23], and vortex-lattice method used by Kagemoto [24], have been used to describe the hydrodynamic performances of fish in applications thus far. However, they are based on potential flow, linearized body boundary conditions, and an assumed wake shape. They neither get the solution of nonlinear flow-body interaction nor allow the coupling wake dynamics to develop [25].

The surrounding fluid must be considered in designing soft robotic fish because it increases mass, stiffness, and damping and changes the mechanical dynamic characteristics of the robot structure. To fully investigate soft robotic fish propulsion performance, we must consider the interaction between the robot structure and fluid



and model the coupling mechanism accurately for fluid-structure interaction (FSI) analysis [26].

With rapid developments in numerical studies, especially computational fluid dynamics (CFD), researchers are applying this numerical method in predicting the hydrodynamic behavior in FSI. To capture the influence of deformed robotic fish on hydrodynamic performance, robot deformation must be passed back as a load into the CFD solution, enabling two-way transfer including structural analysis results between the fluid and structure domain. Fluid loads in structural applications and structural deformation in CFD analysis are considered in FSI. It is widely applied in engineering and biomedicine to solve FSI problems in flexible structures and to predict their hydrodynamic characteristics [27–35]. Although such research provides the basis of flow formulation and boundary conditions of fully FSI analysis, FSI analysis has not been widely applied to the soft robotic fish. Due to the larger flexible structure deformation and complex coupling dynamics with the surrounding fluid, it is difficult to make modeling work and to solve the FSI problems of soft robotic fish. Compared to conventional rigid robotic fish, the soft robot has larger deflection and large deformation is easily generated in interaction with surrounding fluid. Deformation results from soft robots cannot be ignored and problems of mesh motion are easily generated in analysis, which increases the difficulty of solving nonlinear problems in soft robotic fish, especially on the convergence of data transfer and computational cost in soft robot FSI calculation. Although some mesh problems with large deformation are solved by special methods such as grid reconstruction, FSI analysis has not been generally applied to highly nonlinear problems or large deformation problems of soft robot. Good mesh quality at the interface also increases the difficulty of solving mesh problems. There is a challenge on convergence solution in these FSI problems. Besides, the selection of a reasonable and suitable time scale in the computational domain at lower computational cost increases the difficulty of achieving FSI solution of soft robot fish. In FSI analysis, the time scale, which plays the key role in data convergence, depends on fluid force, the scale of wake structures, and the oscillation frequency of soft robots. Fluid force and wake structures differ for different oscillation frequencies. An inappropriate time scale prevents the convergence of calculation for FSI solution of soft robotic fish. An appreciate time scale with low cost is difficult to select in FSI problems of soft robotic fish.

Soft robotic fish considering soft behavior of real fish based on soft material is a young research field in the area of underwater robots. It is going to overcome basic assumptions concerning conventional rigid robots and solid theories and technologies in unknown or dangerous environments. Compared to rigid robots, the theories and technologies of soft robotic fish have not yet been defined in a general form. Design has not been established and research activities are still exploring new ways for improving design and performance of the soft robot. Exact control in path planning and position sensing for soft robotic

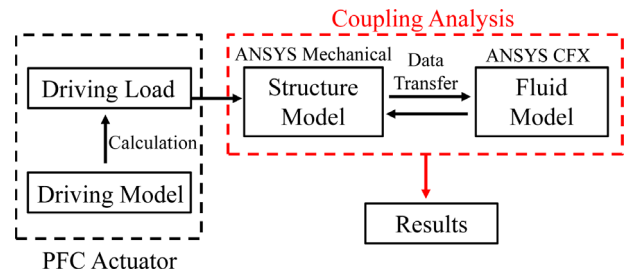


Fig. 1. FSI analysis of soft robotic fish using PFC.

fish as a continuum is complicated in comparison to those of rigid robots. A challenge in design and control exists in high mobility and flexibility of soft robots. This motivates us to investigate the design and control problems of soft robotic fish by using analytical simulation with interaction between the flexible robot structure and fluid.

In the swimming of actual fish, body/caudal fin (BCF) propulsion is more widely used and applied in the design of robotic fish due to its relatively high efficiency, high acceleration, and fast swimming speed. In the present research, we use the PFC as soft actuator to develop soft robotic fish with BCF propulsion. PFC is constructed as a simple structure with a high energy conversion efficiency and a large displacement response. This paper introduces CFD-based FSI analysis to predict and enhance the propulsive force and deformation mode of soft robotic fish. Results of experiments validate its propulsive force and deformation displacement. A comparison of results between experiments and simulation confirmed the effectiveness of FSI analysis and that it is applicable to evaluating the propulsion characteristics of soft robotic fish. In Section 2, it shows the basic FSI analysis scheme and numerical robot structure and surrounding fluid models. Numerical FSI analysis of the soft robot is performed based on these models. Section 3 describes numerical results and a discussion. Section 4 shows our conclusions regarding results.

2. FSI Analysis

2.1. Scheme

When a soft robotic fish comes into contact with a fluid flowing in the direction of oscillation, the robot body may be deformed due to fluid pressure. In return, the deformed robot body changes the fluid flow. In terms of FSI analysis, this deformation results from the robot structure, and fluid pressure loads from the corresponding fluid domain are all considered in the calculation, resulting in two-way data transfer. CFD-based FSI analysis is performed to deal with the FSI problem of the soft robotic fish through ANSYS software. Mechanical application is used for the structure domain and CFX application is used for the fluid domain. Fig. 1 describes the concept of our FSI analysis strategy of soft robotic fish using PFC.

According to the PFC actuator drive model, external

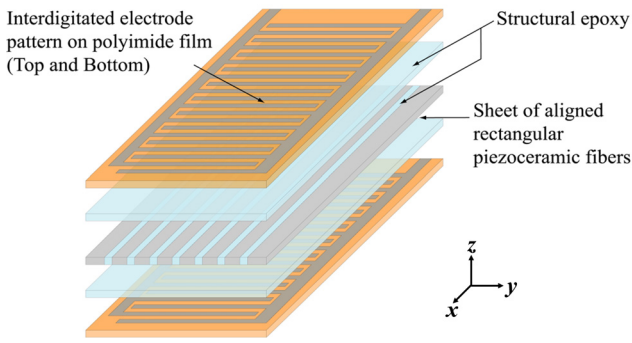


Fig. 2. MFC structure [16].

drive load is calculated and applied to the robot structure model for actuation in the mechanical application based on the calculated result. To solve coupling analysis, the robot structure model with the time-varying drive load is solved first. After the structure model is solved, results such as displacement and stress are exported and these results are converted to input data for the surrounding fluid model in the CFX. To account for the fluid effect, corresponding fluid force loads from the fluid model are converted to the structure model as external load. Interaction between the robot structure model and the fluid model occurs and coupling analysis is developed, enabling propulsion characteristics such as propulsive force and the robotic fish deformation mode in fluid to be exported from simulation results.

2.2. PFC Actuator

We chose macrofiber composite (MFC) – a typical PFC [16], which has a thin plate-like structure – for its large strain response and high efficiency – as a soft actuator. Fig. 2 describes the MFC structure. Piezoceramic fiber is embedded in epoxy to make a rectangular plate. That is then sandwiched between two pieces of polyimide film on which there are interdigitated electrodes.

Applying voltage to MFC causes an internal electric field and polarized crystals cause strain deformation. Expansion and contraction occur in the direction of fibers due to piezoelectricity. When MFC is attached to an elastic plate, this expansion and contraction are transmitted from the fibers to the elastic plate surface, generating structural bending or torsion deformation through piezoelectric strain. Resonant behavior with large displacement is also produced. This structural bending is used to realize propulsion of the soft robotic fish in robot design. To obtain corresponding expansion and contraction in the numerical model, stress caused by piezoelectric strain is defined as external drive load and applied to MFC to reproduce movement to describe its drive characteristics and deformation response. Fig. 3 describes the drive method of stress on MFC to present piezoelectric fiber expansion and contraction. Stress load is applied perpendicularly to the four areas of MFC plates. Positive stress causes contraction and negative stress causes expansion.

According to the elastic constitutive equation of piezo-

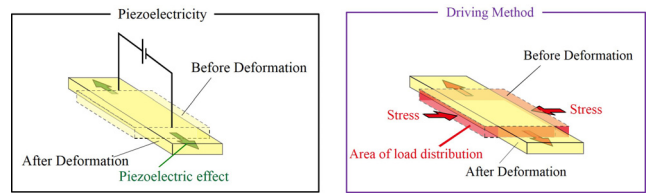


Fig. 3. Drive for MFC.

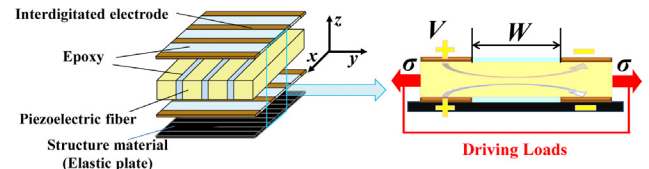


Fig. 4. Basic MFC drive model.

electric material, stress distribution of MFC plate is treated as a plane stress problem because MFC is a thin, planar actuation device. That is, out-of-plane normal and transverse shear stress is considered to be zero [36]. The desired bending of the robot depends mainly on normal stress. The relationship between normal stress and strain in piezoelectric fiber composite is described as indicated by Eq. (1) below using a compliance coefficient matrix [36]. Compliance coefficient matrix *s* is described by Poisson’s ratio *ν* and tensile modulus *E*,

$$\begin{bmatrix} \sigma_x \\ \sigma_y \end{bmatrix} = \begin{bmatrix} s_{xx} & s_{xy} \\ s_{yx} & s_{yy} \end{bmatrix}^{-1} \begin{bmatrix} \epsilon_x \\ \epsilon_y \end{bmatrix} \dots \dots \dots (1)$$

$$s = \begin{bmatrix} \frac{1}{E_x} & -\frac{\nu_{yx}}{E_y} \\ -\frac{\nu_{xy}}{E_x} & \frac{1}{E_y} \end{bmatrix} \dots \dots \dots (2)$$

where ϵ is strain, σ is stress, E_x and E_y are tensile moduli in the *X* and *Y* directions, and ν_{xy} and ν_{yx} are the Poisson’s ratio.

The basic MFC drive model is shown in Fig. 4. When a voltage from -500 V to $+1500$ V is applied to MFC, piezoelectric strain is generated as indicated by Eq. (3). Electric field intensity E_V is calculated using Eq. (4), where V is voltage applied to MFC and W is the distance between MFC electrodes. The stress thus generated is derived from the piezoelectric strain equation, and its calculation equation is described by Eq. (5) based on Eq. (1). The voltage applied for driving is described as generated stress for robot activation in numerical analysis:

$$\begin{bmatrix} \epsilon_x \\ \epsilon_y \end{bmatrix} = \begin{bmatrix} d_{33} \\ d_{31} \end{bmatrix} E_V \dots \dots \dots (3)$$

$$E_V = \frac{V}{W} \dots \dots \dots (4)$$

$$V = W (1 - \nu_{xy}\nu_{yx}) \begin{bmatrix} d_{33} \\ d_{31} \end{bmatrix}^{-1} \begin{bmatrix} E_x & E_x\nu_{yx} \\ E_y\nu_{xy} & E_y \end{bmatrix}^{-1} \begin{bmatrix} \sigma_x \\ \sigma_y \end{bmatrix} \dots \dots \dots (5)$$

Table 1. Material properties of MFC.

Item	Property
Density [kg/m ³]	5440
Tensile modulus E_x [GPa]	30.336
Tensile modulus E_y [GPa]	15.857
Shear modulus [GPa]	5.515
Poisson's ratio ν_{xy}	0.31
Poisson's ratio ν_{yx}	0.16
Piezoelectric constant d_{33} [pm/V]	400 (Low electric field)
	460 (High electric field)
Piezoelectric constant d_{31} [pm/V]	-170 (Low electric field)
	-210 (High electric field)
Distance between the electrodes W [mm]	0.0533
Thickness [mm]	0.3

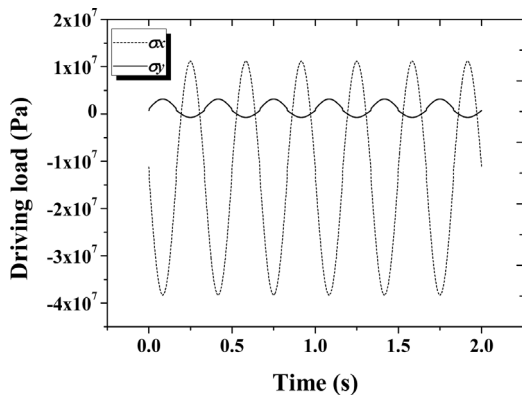


Fig. 5. Drive stress loads of soft robotic fish (3 Hz).

where d_{33} and d_{31} are piezoelectric constants.

Based on the material properties of MFC in **Table 1** [37, a], generated stress is calculated by Eq. (5). The time history of this time-varying stress load is shown in **Fig. 5**, where we take the frequency of 3 Hz in the sine signal waveform as an example of description. Through the loading described in **Fig. 3**, stress loads are applied to the robot structure for activation in analysis. The structure is expanded and contracted in the direction of fibers by the drive load [36]. The desired MFC plate deformation generated is beneficial in the motion design of the soft robotic fish.

Combining MFC with a thin elastic plate results in structural bending deformation. We use this bending deformation to design a robot and to investigate its motion performance. Carbon-fiber-reinforced polymer (CFRP) is used as the thin elastic plate in this research.

2.3. Robot Structure Model

The prototype and geometric model of the soft robot structure are shown in **Fig. 6**. To measure propulsion, fixed support is applied to the robot head in experiments and simulations.

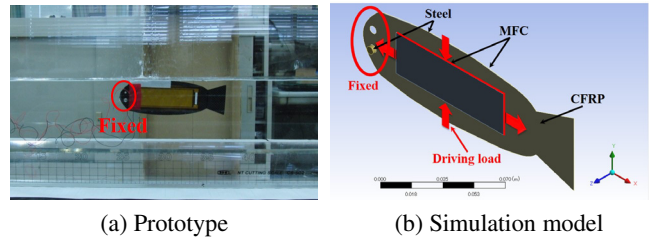


Fig. 6. Soft robotic fish.

Table 2. Material properties of soft robotic fish.

Item	Material	
	Weight	CFRP
Density [kg/m ³]	7850	1700
Elastic modulus [GPa]	20	29.5
Poisson's ratio	0.3	0.3
Thickness [mm]	2.5	0.2

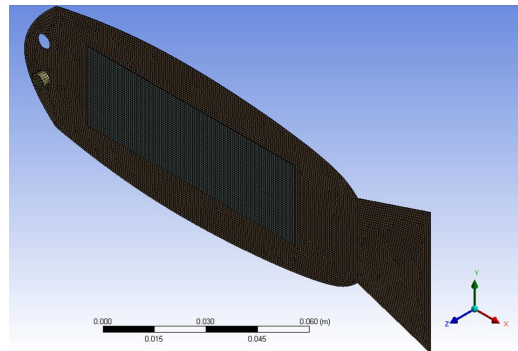


Fig. 7. Finite element model of soft robotic fish.

The robot consists of one CFRP plate and two MFC plates. The two MFC plates sandwich the CFRP plate as the actuator structure for bending deformation propulsion. Steel weight is placed on the head to constrain its movement and to increase tail displacement. This constrained structure is similar to a cantilever. Body height varies toward the tail and is smallest where the caudal fin is connected to the body. In experiments, a low-density blowing agent acting as float adheres on the top of the robot to balance and stabilize robot weight. MFC with M-8528-P1 is used [a], and voltage from -500 V to +1500 V is applied to activate the robot in experiments and simulation. Using this drive load generates bending deformation and the robot oscillates in the direction of the Z-axis. The robot is 167 mm long. Material properties of the robot structure are shown in **Table 2**.

The finite element model of the soft robot structure shown in **Fig. 7** is described by a hexahedral element. Grid nodes number 152,902 and elements 28,181.

Based on a finite element model of the soft robotic fish, fixed support is applied to the robot head and drive load from Eq. (5) is applied to areas of two MFC plates for activation described in **Fig. 6(b)**. When an external force is applied to the end of the rod, force is transferred equally

across the rod. Force is the factor causing stress. Stress defined as force acting on unit area within a deformable body is applied to MFC plate area where net force is normal to the plane of the area considered. Only one MFC plate's load distribution is obtained in Fig. 6(b). The drive load for the other MFC plate is applied in the opposite direction based on corresponding areas of load distribution. The basic governing finite element matrix equation of the soft robot structure is as follows [38]:

$$M\ddot{X} + C\dot{X} + KX = F_R \quad F_R = f_b + f_F \quad \dots \quad (6)$$

$$f_b = \int_B \sigma_i n_i dB \quad \dots \quad (7)$$

$$f_F = \int_S P n_j dS + \int_S \tau n_j dS \quad \dots \quad (8)$$

where M , C and K are structural element mass, damping and the stiffness matrix. F_R is force applied to the structure, including external force f_b and force f_F describing coupling to surrounding fluid. X is displacement, σ_i is generated actuator stress, and n_i is the i -th component of the unit normal vector in the area of dB , where B is the area of load distribution on the MFC plate. P is fluid pressure, τ is the fluid shear stress related to fluid viscosity and shear rate, n_j is the j -th component of the unit normal vector on the surface area of the interface boundary, and S is the surface area of the robot.

In FSI of soft robotic fish, f_b characterizes external force load acting on the robot structure for activation. The voltage described in the form of generated stress of MFC actuator is defined as the robot's external drive load and is calculated using Eq. (5) based on MFC's material properties. Applied stresses are normal to the plane of MFC actuator area considered. External force load f_b is described as in Eq. (7), related to generated stress of actuators. f_F characterizes the force load caused by surrounding fluid acting on the robot structure. It includes fluid pressure force and shear stress. The robot is thus subjected to fluid force load at the interface boundary between the surrounding fluid and robot structure and f_F is described as in Eq. (8). Any fluid viscosity force or fluid friction force acting on the robot structure is included in f_F but not in damping matrix C described in Eq. (6) for the FSI solution. Fluid force load is generated in interaction between the robot structure and the surrounding fluid. Load transfer occurs on the interface between them. Through this interface boundary, fluid force load is transferred to the robot structure. Force load caused by fluid is thus applied to the interface area of the robot structure in calculation. That is, fluid force load is applied to the entire surface of the robot structure for the FSI solution.

2.4. Fluid Model

3-D incompressible Navier-Stokes equations and continuity equations used to model the surrounding fluid domain described in Fig. 8 are shown below and are solved by using the finite volume method. Using these equations with additional boundary conditions solves nonlinear problems and describes the distribution of fluid veloc-

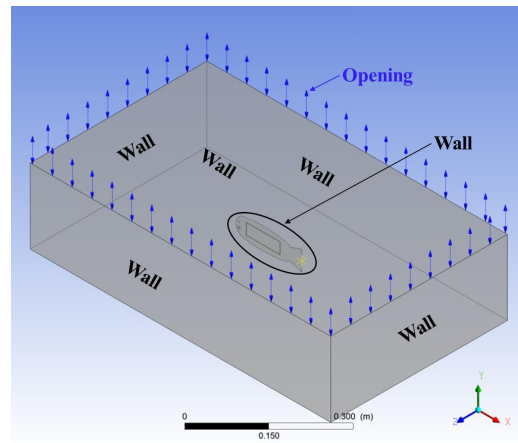


Fig. 8. Fluid model boundary conditions.

ity and pressure around the soft robotic fish. To obtain a time-unsteady solution using a relatively simply solver at lower computational cost, the additional turbulence model is used as a simplified, approximate model so that approximate modeling of the fluid in analysis has the difference with real conditions in practice. It can, however, be employed to calculate complex flow with high Reynolds numbers and meet the basic demands of the physics of turbulent flow:

$$\rho \left(\frac{\partial U_x}{\partial t} + U_x \frac{\partial U_x}{\partial x} + U_y \frac{\partial U_x}{\partial y} + U_z \frac{\partial U_x}{\partial z} \right) = \mu \left(\frac{\partial^2 U_x}{\partial x^2} + \frac{\partial^2 U_x}{\partial y^2} + \frac{\partial^2 U_x}{\partial z^2} \right) - \frac{\partial P}{\partial x} + F_x \quad \dots \quad (9)$$

$$\rho \left(\frac{\partial U_y}{\partial t} + U_x \frac{\partial U_y}{\partial x} + U_y \frac{\partial U_y}{\partial y} + U_z \frac{\partial U_y}{\partial z} \right) = \mu \left(\frac{\partial^2 U_y}{\partial x^2} + \frac{\partial^2 U_y}{\partial y^2} + \frac{\partial^2 U_y}{\partial z^2} \right) - \frac{\partial P}{\partial y} + F_y \quad \dots \quad (10)$$

$$\rho \left(\frac{\partial U_z}{\partial t} + U_x \frac{\partial U_z}{\partial x} + U_y \frac{\partial U_z}{\partial y} + U_z \frac{\partial U_z}{\partial z} \right) = \mu \left(\frac{\partial^2 U_z}{\partial x^2} + \frac{\partial^2 U_z}{\partial y^2} + \frac{\partial^2 U_z}{\partial z^2} \right) - \frac{\partial P}{\partial z} + F_z \quad \dots \quad (11)$$

$$\nabla \cdot U = \frac{\partial U_x}{\partial x} + \frac{\partial U_y}{\partial y} + \frac{\partial U_z}{\partial z} = 0 \quad \dots \quad (12)$$

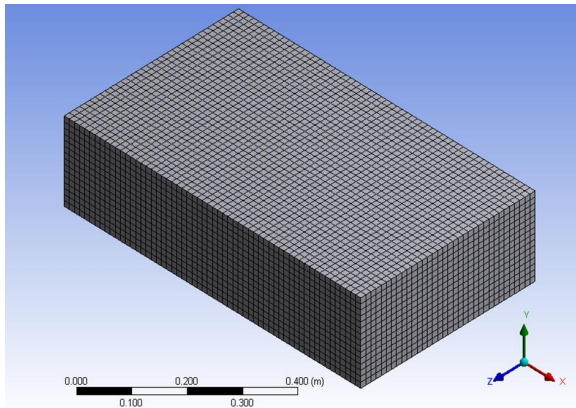
where ρ is density, U is velocity, U_x , U_y and U_z are velocity components in the X , Y , and Z directions, P is pressure, μ is dynamic viscosity, and F_x , F_y and F_z are force components in the X , Y , and Z directions.

As shown in Fig. 8, a cubic surface is the fluid domain boundary, which is $590 \times 133 \times 440$ mm, the same as the liquid tank in experiments. The soft robotic fish is centered in the transverse and vertical directions of the fluid domain.

Due to the high voltage of MFC, fully fluorinated and thermally stable Fluorinert electronic liquid FC3283 is used to describe properties of the fluid in Table 3. FC3283 has good electrical insulation properties, meeting insulat-

Table 3. Fluid properties.

Item	Property
Density (kg/m^3)	1820
Average Molecular Weight (g/mol)	521
Kinematic Viscosity (centistokes)	0.75
Absolute Viscosity (centipoises)	1.4

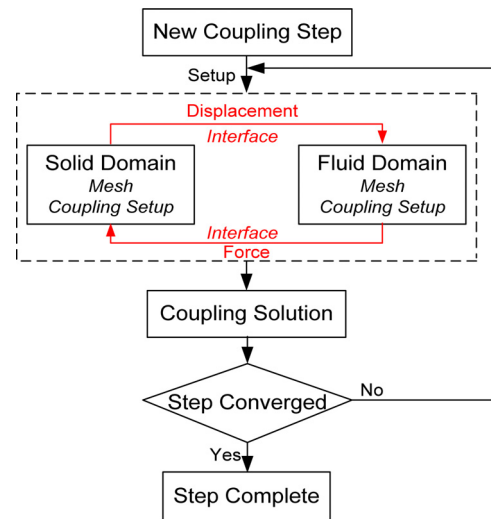
**Fig. 9.** Fluid model mesh.

ing requirements in experiments. Its composition does not shift or fractionate over time, which insures that fluid transport properties are stable. It is also nontoxic orally, nonflammable, and highly resistant, increasing security in storage and use.

The fluid model has some basic conditions. First, the standard atmosphere and 25°C room temperature are presented as reference values. Second, buoyancy and heat transfer are not considered. Buoyant force perpendicular to the direction of robot locomotion has almost no effect on propulsion. Heat transfer in the fluid has little effect on energy dissipation in propulsion and is ignored for reasons of simplification in research. Third, the shear-stress transport (SST) equation model is defined as a fluid turbulence model that considers the transport of turbulent shear stress and predicts fluid flow on a curved surface and separated flow on boundary layers accurately enough to represent turbulence flow physics in calculation.

Two of the boundary conditions in **Fig. 8**, that is, opening and the nonslip wall boundary, are applied to model the fluid domain in simulation. The nonslip wall boundary condition is applied to the entire interface of robot structure and the borders of the fluid domain expect for the border of top surface. Fluid velocity on the wall boundary is zero. The top surface of the fluid domain is described by an opening boundary condition on which pressure with a zero value is applied.

The fluid model's mesh grids, shown in **Fig. 9**, are meshed through the ANSYS mesh method. The element type is hexahedral. Fluid model grid nodes number 105,136 and elements number 533,943. Mesh distribution from the robot surface to the fluid border is sparse. The

**Fig. 10.** Solution procedure of FSI analysis.

density of the grid nodes on the robot surface is largest in the fluid model.

2.5. Numerical Coupling Analysis

Transient analysis is used in both the structure and fluid model to determine hydrodynamic performance of soft robot in coupling simulation. FSI analysis through the ANSYS program assumes that fluid is ideal and meets basic conditions. First, the solid structure has large flexible deflection. Second, the fluid is nonflowing. Third, there is no heat transfer process and no buoyancy is considered in analysis. Initial values for all variables needed in the analysis are defined as zero.

Interaction between the robot structure and fluid at the interface causes the fluid to exert force on the robot and structure motion produces an effective fluid load. The governing equations of the robot structure and fluid domain are coupled by fluid-structure interfacial boundary conditions. FSI analysis meets basic principles of continuity and the conservation of velocity, stress, displacement, heat flow, and temperature at the interface between them. The detailed solution procedure for FSI analysis between the robot structure and fluid is shown in **Fig. 10**. The solid domain and fluid domain have separate mesh distribution and boundary conditions in analysis. Data is transferred on the interface between the solid and fluid domains. Each field solvers gather required transfer data from the other solvers, solving their equations for the current coupling step. Step calculation is repeated until data transfer between two solvers and all field equations have converged. After convergence, current coupling calculation moves to the next step in analysis. Transferred data in FSI analysis of soft robotic fish are force from the fluid and displacement from the robot structure.

To evaluate soft robotic fish's hydrodynamic performance, the propulsive force of the robot is derived from 3-D computation. When oscillation and swimming velocities of the soft robotic fish are determined, the robot's

hydrodynamic force is related only to fluid pressure and viscous stress over the robot surface. At a defined oscillation frequency, oscillation and swimming velocities are determined and corresponding fluid pressure and viscous stress caused by the swimming motion of soft robotic fish are obtained in FSI analysis. In simulation, the robot oscillates in the Z-axis direction at a defined oscillation frequency and hydrodynamic force along the X-axis is considered only for propulsion. At different oscillation frequencies, the hydrodynamic force component along the X-axis is calculated as the integral of pressure and viscous stress over the robot surface in the X-axis direction, shown in Eq. (13) [39]:

$$F_x = \oint_A (-\vec{P} \cdot \vec{n}_x + \vec{\tau}_{xj} \cdot \vec{n}_j) dA \quad \dots \quad (13)$$

where dA is the infinitesimal robot surface area, P is the pressure of area dA , n_j is the j -th component of the unit normal vector of area dA , n_x is the unit normal vector of area dA in the X-axis direction, and τ_{xj} is the viscous stress tensor of area dA in the X-axis direction.

3. Results and Discussion

According to the above boundary conditions and properties of fluid, FSI simulation is conducted to determine the soft robotic fish's hydrodynamic performance. Propulsive force and deformation mode play crucial roles in soft robotic fish's propulsion, so results of propulsive force and deformation displacement of the soft robotic fish are presented below.

3.1. Propulsive Force

Fluid pressure plays a key role in soft robot fish's propulsion. Based on the robot's specific oscillation frequency, pressure distribution around the robot varies with time. **Fig. 11** shows fluid pressure on the X-Z midplane in a half cycle at 3 Hz. Here we use pressure relative to one standard atmosphere to express static pressure in the fluid.

As shown in **Fig. 11**, the robot oscillates. The pressure of the flow field near the robot is obviously disturbed and dynamic pressure is determined by robot motion. Pressure contours crowd close together near the robot, where the higher pressure is obtained. The pressure peak and trough appear at the tail of the robot, which is where the robot is deformed the most. Due to robot oscillation, an obvious pressure differential is generated at left and right around the robot. The pressure difference between the front and back of the robot is very low, benefitting from its streamlined shape. **Fig. 11(b)** shows fluid pressure where the robot is most deformed. As the robot increasingly deforms, the area of fluid disturbance expands.

Hydrodynamic force results along the X-axis are shown in **Fig. 12**. The input voltage of the square waveform on the robot ranged from -500 V to $+1500$ V and the range of frequency is 1 Hz to 25 Hz in experiments and simulation. The experimental platform on propulsive force

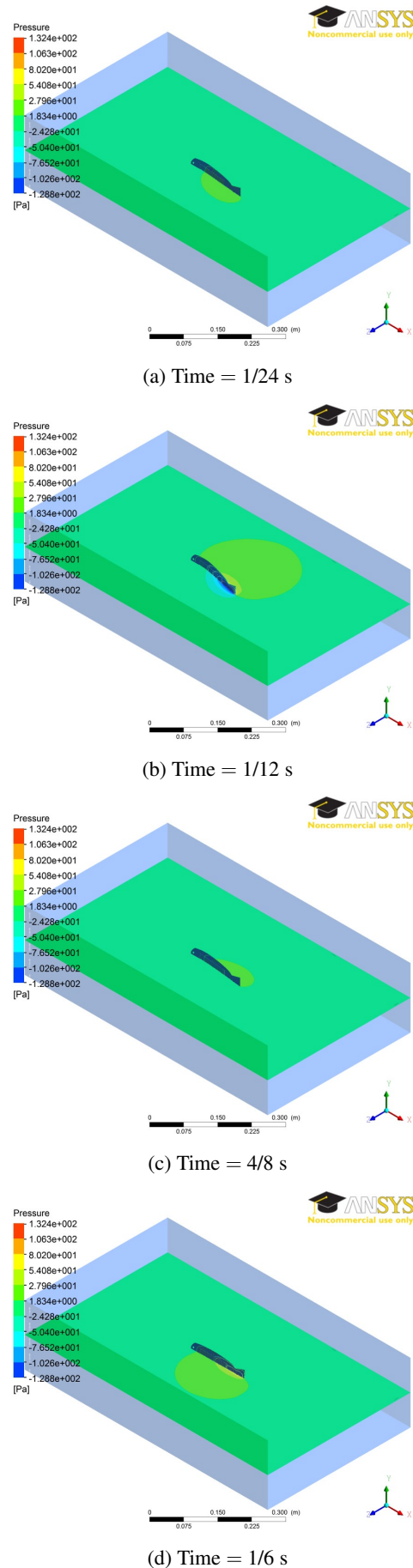


Fig. 11. Fluid pressure contours on the X-Z midplane in a half cycle at 3 Hz.

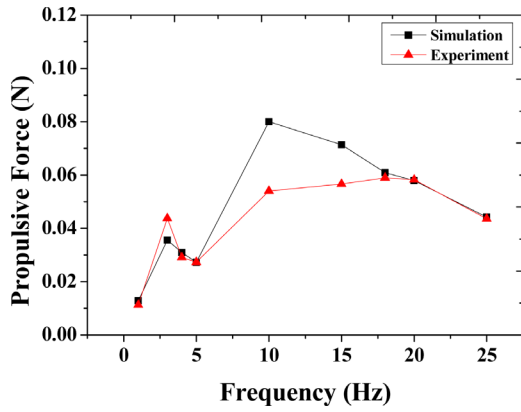


Fig. 12. Propulsive force of soft robotic fish in experiments and simulations.

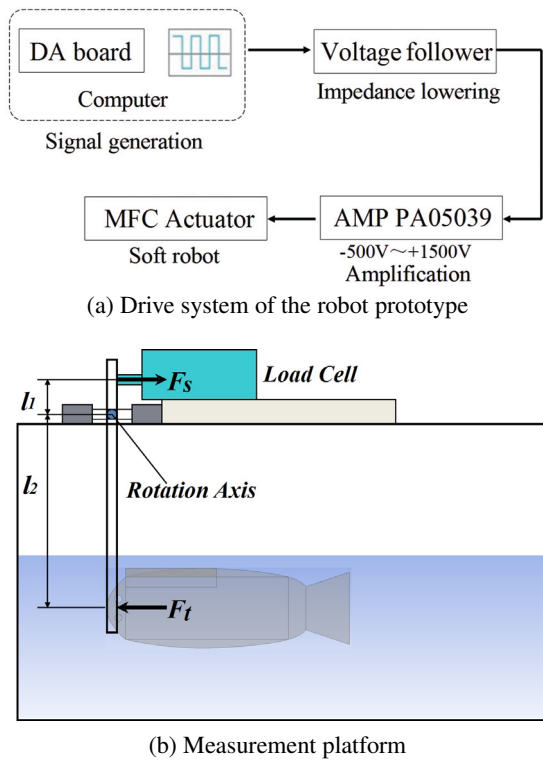


Fig. 13. Experimental propulsive-force platform.

is shown in Fig. 13, including the prototype drive system. Main drive signal generation is computer-controlled and the basic signal waveforms such as sine, square and triangle are considered. The signal processing circuit uses a voltage follower between the high-voltage amplifier (AMP PA05039) and the computer to reduce output impedance. The high-voltage amplifier delivers an output voltage of -500 V to $+1500\text{ V}$ at an output current up to 50 mA . DC is used to drive MFCs. High-voltage output is controlled through the amplifier input voltage of -2.5 V to 7.5 V DC or peak AC corresponds to -500 V to $+1500\text{ V}$ output.

In experiments, measurement is performed in the Fluorinert electronic liquid tank, which is $590 \times 133 \times 440\text{ mm}$ due to the high input voltage of actuators. The force gauge

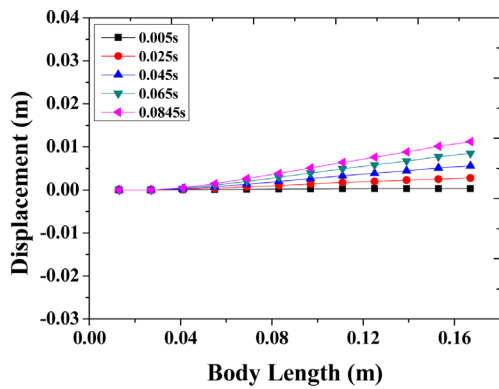
(single-axis load cell) and a stick are used to build the experimental platform. The force gauge is fixed on the upper part of stick. The stick rotates with the rotation axis. The lower part of stick contacts to the robot prototype head. When input voltage is applied to the robot, the robot generates force for propulsion and the stick contacting the robot head rotates with the rotation axis. Through the rotation axis, propulsive force is transferred to the upper part of stick. Based on force F_s from the load cell fixed on the upper part of stick, the prototype's propulsive force F_t is calculated by Eq. (14). The distance between the rotation axis and the upper part of stick, where the stick is fixed on the force gauge, is l_1 and the distance of the rotation axis away from the lower part of stick where the stick contacts the robot is l_2 . Propulsive force is the value averaged in measured time.

$$F_t = \frac{l_1 F_s}{l_2} \dots \dots \dots (14)$$

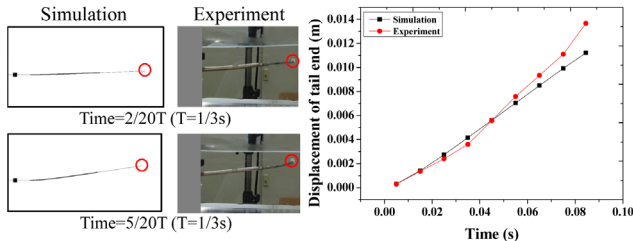
In Fig. 12, no direct proportional relationship exists between propulsive force and robot oscillation frequency, but similar variations in propulsive force happen in experiments and simulation. Due to the fluid model and boundary conditions in simulation, force differs largely in a frequency range from 10 Hz to 18 Hz . In simulation, the numerical fluid model is modelled to represent approximately turbulent flow physics for the FSI solution. Many parameters in governing equations of the fluid model are determined by experience. This approximate fluid model reduces simulation accuracy and causes a difference in fluid flow compared to actual conditions. Real turbulent flow physics are not described accurately. Load acting on the robot structure caused by fluid is all an approximate solution and causes error between simulated and measured results. In numerical analysis, the uniform fluid model and boundary condition are selected to avoid systematic error. In this frequency range, the uniform fluid model and boundary conditions cause large differences. Compared to real conditions in experiments, the simplified model including the fluid and robot structure and boundary conditions in numerical analysis are another source of differences. Experimental measurement from a fixed device and hand-made error in prototype manufacture also cause the difference between experiments and simulation. In conclusion, similar results occur in experiments and simulation. Trends in variations in propulsive force of the soft robotic fish at different frequencies is determined and results similar to experiments are obtained through FSI analysis.

3.2. Deformation Displacement of Soft Robotic Fish

Corresponding deformation modes of soft robotic fish at different frequencies are also obtained from FSI analysis. At different frequencies, we obtain similar bending deformation modes in the robot propulsion. We take the results at 3 Hz where the robot has good flexible fish-like motion due to suitable swimming number S_w [40] to present its bending deformation mode, shown in Fig. 14. Results for a quarter of one cycle are used for description.



(a) Simulation results of deformation mode



(b) Displacement comparison between experiments and simulation

Fig. 14. Deformation mode of soft robotic fish in one quarter of a cycle at 3 Hz.

Fig. 14(b) describes the difference in deformation mode between experiments and simulation at 3 Hz. Experimental results are measured by a high-speed camera.

As shown in **Fig. 14**, the bending deformation mode occurs in robot oscillation, and deformation displacement is increasing gradually from 0.005 s to 0.0845 s at 3 Hz. At 0.0845 s, the deformation reaches the maximum. At different time values, maximum deformation is obtained at the caudal fin end as shown in **Fig. 14(a)**. Almost the same bending mode shapes occur at corresponding time values in experiments and simulation, as shown in **Fig. 14(b)**. At left are bending mode shapes in experiments and simulation. At right are corresponding displacement differences of the tail end. At 3 Hz, the maximum displacement difference at the tail end is 18% between them. Efficient bending propulsion based on oscillation is thus realized successfully through FSI analysis.

Results on caudal fin displacement at different frequencies are shown in **Fig. 15**. Note the similar displacement curve in experiments and simulation. Maximum displacements in the experiments and simulation are obtained at 1 Hz rather than at the frequency where the maximum propulsive force is generated because fluid absorbs energy from resonance and resonance energy is not transferred completely to the robot. At 1 Hz, maximum displacement is 24.7 mm in experiments and 34 mm in simulation, yielding a maximum displacement difference of 39%. Simulation results in tail displacement are close to those from experiments. The effectiveness of FSI analysis is thus verified and suitable for evaluating deformation characteristics of soft robotic fish in propulsion.

Propulsive force and the deformation trajectory are estimated for soft robotic fish at different frequencies in FSI

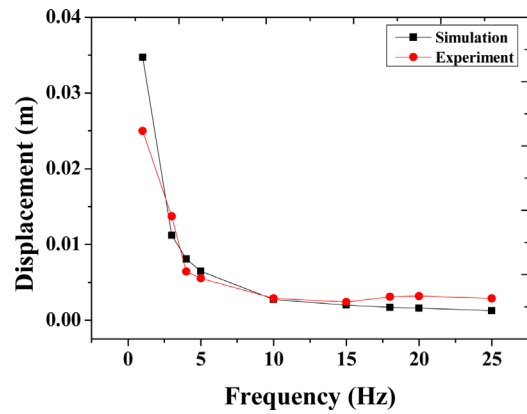


Fig. 15. Displacement of caudal fin end in experiments and simulation.

simulation. FSI analysis meets the initial demands of soft robotic fish design and control from the view of morphology. From the view of dynamics, however, differences in propulsive force and deformation displacement exist in experiments and simulation. The float on the robot is a key factor causing these differences. The presence of the float changes the flow field distribution in robot oscillation. Hand-made error from manufacture and experimental measurement on prototypes is another source of differences. We will consider them in the further improvement. As a conclusion, simulation results for propulsive force and deformation mode coincide with experimental results. The effectiveness of FSI analysis has been verified by comparing experiments. Design and control based on FSI analysis is used to evaluate soft robotic fish's propulsion performance to further improve.

4. Conclusions

FSI analysis has been used to evaluate propulsion characteristics of soft robotic fish using PFC for robot design and control. Propulsive force and deformation trajectories of soft robotic fish are estimated through FSI analysis. A comparison of results between experiments and simulation has verified the effectiveness of FSI analysis of soft robotic fish and shown FSI analysis to be suitable for evaluating soft robot fish's propulsion performance for further optimization and improvement. In future, we plan to design insulating packages of soft robots and use FSI analysis to develop new robotic fish with advanced propulsion performance.

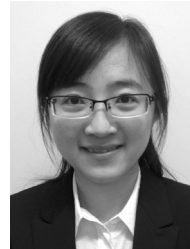
References:

- [1] E. Kim and Y. Youm, "Design and dynamic analysis of fish robot: PoTuna," Proc. of IEEE Int. Conf. on Robotics and Automation, pp. 4887-4892, 2004.
- [2] J. M. Anderson, "The vorticity control unmanned undersea vehicle," Proc. of Int. Symposium on Seawater Drag Reduction, pp. 479-483, 1998.
- [3] X. Deng and S. Avadhanula, "Biomimetic micro underwater vehicle with oscillating fin propulsion: system design and force measurement," Proc. of IEEE Int. Conf. on Robotics and Automation, pp. 3312-3317, 2005.

- [4] J. M. Kumph, "Maneuvering of a robotic pike," M. S. Thesis, Massachusetts Institute of Technology, USA, 2000.
- [5] M. S. Triantafyllou, A. H. Techet, and F. S. Hover, "Review of experiment work in biomimetic foils," *IEEE J. of Oceanic Engineering*, Vol.29, No.3, pp. 585-593, 2004.
- [6] K. H. Low, C. W. Chong, and C. Zhou, "Performance study of a fish robot propelled by a flexible caudal fin," *Proc. of IEEE Int. Conf. on Robotics and Automation*, pp. 90-95, 2010.
- [7] X. Tan, M. Carpenter, J. Thon, and F. Alequin-Ramos, "Analytical modeling and experimental studies of robotic fish turning," *Proc. of IEEE Int. Conf. on Robotics and Automation*, pp. 102-108, 2010.
- [8] A. Crespi, A. Badertscher, A. Guignard, and A. J. Iispeert, "Amphibot I: an amphibious snake-like robot," *Robotics and Autonomous Systems*, Vol.50, pp. 163-175, 2005.
- [9] H. Hu, "Biologically inspired design of autonomous robotic fish at Essex," *Proc. of IEEE SMC UK-RI Chapter Conf. on Advances in Cybernetic Systems*, pp. 1-8, 2006.
- [10] S. Hirose and E. F. Fukushima, "Snakes and strings: new robotic components for rescue operations," *Int. J. of Robotics Research*, Vol.23, pp. 341-349, 2004.
- [11] M. Mojarad and M. Shahinpoor, "Biomimetic robotic propulsion using polymeric artificial muscles," *Proc. of IEEE Int. Conf. on Robotics and Automation*, pp. 2152-2157, 1997.
- [12] Z. Zhang, N. Yamashita, and M. Gondo, "Electrostatically actuated robotic fish: design and control for high-mobility open-loop swimming," *IEEE Trans. on Robotics*, Vol.24, No.1, pp. 118-129, 2008.
- [13] S. Guo, Y. Ge, L. Li, and S. Liu, "Underwater swimming micro robot using IPMC actuator," *Proc. of IEEE Int. Conf. on Mechatronics and Automation (ICMA)*, pp. 249-254, 2006.
- [14] O. K. Rediniotis, L. N. Wilson, D. C. Lagoudas, and M. M. Khan, "Development of a Shape-Memory-Alloy actuated biomimetic hydrofoil," *J. of Intelligent Material Systems and Structures*, Vol.13, No.1, pp. 35-49, 2002.
- [15] T. Fukuda and H. Hosokai, "Giant magnetostrictive alloy (GMA) application to micro mobile robot as a micro actuator without power supply cable," *Proc. of IEEE Int. Conf. on Micro Electro Mechanical System (MEMS)*, pp. 210-215, 1991.
- [16] R. B. Williams and D. J. Inman, "An overview of composite actuators with piezoceramic fibers," *Proc. of 20th Int. Modal Analysis Conf.*, pp. 421-427, 2002.
- [17] K. H. Low and A. Willy, "Biomimetic motion planning of an undulating robotic fish fin," *J. of Vibration and Control*, Vol.12, No.12, pp. 1337-1359, 2006.
- [18] L. Jia and X. Yin, "Passive oscillations of two tandem flexible filaments in a flowing soap film," *Physical review letters*, Vol.100, No.22, pp. 1-4, 2008.
- [19] D. Xia, J. Liu, W. Cheng, and L. Han, "Numerical simulation of the hydrodynamics of fishlike robot swimming based on converged speed," *J. of Mechanical Engineering*, Vol.46, No.1, pp. 48-54, 2010.
- [20] T. Y. Wu, "Hydrodynamics of swimming propulsion. Part 1. Swimming of a two-dimensional flexible plate at variable forward speeds in an inviscid fluid," *J. of Fluid Mechanics*, Vol.46, No.2, pp. 337-355, 1971.
- [21] M. Lighthill, "Large amplitude elongated-body theory of fish locomotion," *Pro. R. Soc. London, Ser. B*, Vol.179, pp. 125-138, 1971.
- [22] J. N. Newman, "The force on a slender fish-like body," *J. of Fluid Mechanics*, Vol.58, No.4, pp. 689-702, 1973.
- [23] J. Cheng, L. Zhuang, and B. Tong, "Analysis of swimming three-dimensional waving plates," *J. of Fluid Mechanics*, Vol.232, pp. 341-355, 1991.
- [24] H. Kagemoto, M. J. Wolfgang, D. K. P. Yue, and M. S. Triantafyllou, "Force and power estimation in fish-like locomotion using a vortex-lattice method," *J. of Fluids Engineering*, Vol.122, No.2, pp. 239-253, 2000.
- [25] H. Liu and K. Kawachi, "A numerical study of undulatory swimming," *J. Comput. Phys.*, Vol.155, No.2, pp. 223-247, 1999.
- [26] H.-J. Bungartz and M. Schäfer, "Fluid-structure interaction: modelling, simulation, optimization," Springer-Verlag, 2006.
- [27] W. Dettmer and D. Peric, "A computational framework for fluid-structure interaction: finite element formulation and applications," *Computer Methods in Applied Mechanics and Engineering*, Vol.195, pp. 5754-5779, 2006.
- [28] S. Gong, L. Ren, H. Liu, L. Li, and Z. Zou, "Fluid-solid interaction of rotor blade in last stage of steam turbine," *Thermal Turbine*, Vol.36, No.3, pp. 153-157, 2007.
- [29] D. Tang, C. Yang, S. Kobayashi, and D. N. Ku, "Effect of a lipid pool on stress/strain distributions in stenotic arteries: 3-D fluid-structure interactions (FSI) models," *J. Biomech. Eng.*, Vol.126, No.3, pp. 363-370, 2004.
- [30] D. Tang, C. Yang, S. Mondal, F. Liu, G. Canton, T. Hatsukami, and C. Yuan, "A negative correlation between human carotid atherosclerotic plaque progression and plaque wall stress: in vivo MRI-based 2D/3D FSI models," *J. Biomech.*, Vol.41, No.4, pp. 727-736, 2008.
- [31] J. Leach, V. Rayz, M. Mofrad, and D. Saloner, "An efficient two-stage approach for image-based FSI analysis of atherosclerotic arteries," *Biomech. Model Mechanobiol*, Vol.9, No.2, pp. 213-223, 2010.
- [32] H.-J. Bungartz, M. Mehl, and M. Schäfer, "Fluid-structure interaction II: modelling, simulation, optimization," Springer-Verlag, 2010.
- [33] H. Schmucker, F. Flemming, and S. Coulson, "Two-way coupled fluid structure interaction simulation of a propeller turbine," *The 25th IAHR Symposium on Hydraulic Machinery and Systems/ IOP Conf. Series: Earth and Environmental Science*, Vol.12, No.1, pp. 1-10, 2010.
- [34] R. L. Campbell, "Fluid-structure interaction and inverse design simulations for flexible turbomachinery," *Doctoral Dissertation of the Pennsylvania State University*, 2010.
- [35] M. Hsu and Y. Bazilevs, "Fluid-structure interaction modeling of wind turbines: simulating the full machine," *Computational Mechanics*, Vol.50, No.6, pp. 821-833, 2012.
- [36] R. B. Williams, "Nonlinear mechanical and actuator characterization of piezoelectric fiber composites," *Doctoral Dissertation of Virginia Polytechnic Institute and State University*, 2004.
- [37] J. W. High and W. K. Wilkie, "Method of fabricating NASA-standard macro-fiber composite piezoelectric actuators," *NASA/TM-2003-212427*, Langley Research Center, Hampton, Virginia, 2003.
- [38] ANSYS Inc., "ANSYS theory reference 12.1," ANSYS Inc., 2009.
- [39] I. Borazjani and F. Sotiropoulos, "Numerical investigation of the hydrodynamics of carangiform swimming in the transitional and inertial flow regimes," *J. of Experimental Biology*, Vol.211, pp. 1541-1558, 2008.
- [40] I. Tanaka and M. Nagai, "Hydrodynamic of resistance and propulsion-learn from the fast swimming ability of aquatic animals," *Ship & Ocean Foundation*, pp. 14-19, 1996.

Supporting Online Materials:

- [a] Smart Material, 2012. <http://www.smart-material.com> [Accessed February 2012]



Name:

Wenjing Zhao

Affiliation:

Department of Mechanical Engineering and Intelligent Systems, The University of Electro-Communications

Address:

1-5-1 Chofugaoka, Chofu-shi, Tokyo 182-8585, Japan

Brief Biographical History:

2007 Received B.S. degree from University of Electronic Science and Technology of China
 2010 Received M.S. degree from University of Electronic Science and Technology of China
 2011- Ph.D. Student, The University of Electro-Communications

Main Works:

- "Dynamic Analysis and Optimization of Soft Robotic Fish Using Fluid-Structural Coupling Method," *Proc. Of the IEEE Int. Conf. on Robotics and Automation*, pp. 1474-1479, 2014.



Name:
Aiguo Ming

Affiliation:
Professor, Department of Mechanical Engineering and Intelligent Systems, The University of Electro-Communications

Address:

1-5-1 Chofugaoka, Chofu-shi, Tokyo 182-8585, Japan

Brief Biographical History:

1990 Received Ph.D. from The University of Tokyo
1990- Joined Mitutoyo Corporation
1991- Joined Yamanashi University
1994- Joined The University of Electro-Communications

Main Works:

- “Biologically Inspired Robotics: Chapter 4 Human-Inspired Hyperdynamic Manipulation,” Y. Liu and D. Sun (Eds.), TAYLOR & FRANCIS, 2011.
- “Development of A Mobile Manipulator System With RFID-Based Sensor Fusion For Home Service: A Case Study on Mobile Manipulation of Chairs,” Int. J. of Information Acquisition, Vol.7, No.1, pp. 1-13, 2010.

Membership in Academic Societies:

- The Institute of Electrical and Electronics Engineers (IEEE)
- The Robotics Society of Japan (RSJ)
- The Japan Society for Precision Engineering (JSPE)
- The Japan Society of Mechanical Engineers (JSME)
- The Society of Instrument and Control Engineers (SICE)



Name:
Makoto Shimojo

Affiliation:
Professor, Department of Mechanical Engineering and Intelligent Systems, The University of Electro-Communications

Address:

1-5-1 Chofugaoka, Chofu-shi, Tokyo 182-8585, Japan

Brief Biographical History:

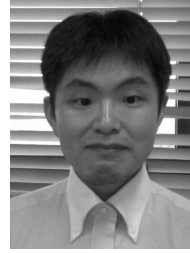
1976-1992 Senior Researcher, Industrial Products Research Institute
1993-1997 Senior Researcher, National Institute of Bioscience and Human Technology
1985-1986 Visiting Scholar, Stanford University
1997-2001 Professor, Computer and Information Sciences, Ibaraki University
2001- Professor, The University of Electro-Communications

Main Works:

- M. shimojo, M. shinohara, and Y. fukui, “Human Shape Recognition Performance for 3D Tactile Display,” IEEE Trans. on Systems, Man and Cybernetics, Part A, Vol.29, No.6, pp. 637-644, 1999.
- M. Shimojo, A. Namiki, M. Ishikawa, R. Makino, and K. Mabuchi, “A tactile sensor sheet using pressure conductive rubber with electrical-wires stitched method,” IEEE Trans. Sensors, Vol.5, No.4, pp. 589-596, 2004.

Membership in Academic Societies:

- The Robotics Society of Japan (RSJ)
- The Society of Instrument and Control Engineers (SICE)
- The Japan Society of Mechanical Engineers (JSME)
- The Virtual Reality Society of Japan (VRSJ)
- The Electronics, Information and Communication Engineers (IEICE)



Name:
Yohei Inoue

Affiliation:
Assistant Professor, Department of Mechanical Engineering and Intelligent Systems, The University of Electro-Communications

Address:

1-5-1 Chofugaoka, Chofu-shi, Tokyo 182-8585, Japan

Brief Biographical History:

2007 Received Ph.D. degree from Osaka University
2007- Postdoctoral Research Fellow, Nagoya Institute of Technology
2011- Postdoctoral Research Fellow, Doshisha University
2011- Assistant Professor, Doshisha University
2013- Assistant Professor, The University of Electro-Communications

Main Works:

- “Numerical simulation of fluid induced vibration of graphenes at micron scales,” CMES, Vol.63, No.2, pp. 137-161, 2010.

Membership in Academic Societies:

- The Japan Society of Mechanical Engineers (JSME)
- The Japan Society of Fluid Mechanics (JSFM)
- The Japanese Society for Multiphase Flow (JSMF)



Name:
Hiroshi Maekawa

Affiliation:
Professor, Department of Mechanical Engineering and Intelligent Systems, The University of Electro-Communications

Address:

1-5-1 Chofugaoka, Chofu-shi, Tokyo 182-8585, Japan

Brief Biographical History:

1981 Received Ph.D. degree from The University of Tokyo
1988- Associate Professor, Faculty of Engineering Kagoshima University
1991- Associate Professor, The University of Electro-Communications
2002- Professor, Hiroshima University
2008- Professor, The University of Electro-Communications
2014- Visiting Professor, Stanford University

Main Works:

- High-resolution numerical schemes for compressible flow
- Compressible Turbulence and Transition to Turbulence
- Computational Aeroacoustics

Membership in Academic Societies:

- The American Institute of Aeronautics and Astronautics (AIAA)
- The Japan Society of Mechanical Engineers (JSME)
- The Japan Society of Fluid Mechanics (JSFM)
- Heat Transfer Society of Japan
- The Visualization Society of Japan
- Turbomachinery Society of Japan